J. Fluid Mech. (1984), *vol.* 140, *pp.* 257–280
Printed in Great Britain

On the interaction of compliant coatings with boundary-layer flows

By MOHAMED GAD-EL-HAK, RON F. BLACKWELDER† AND JAMES J. RILEY‡

Flow Research Company, 21414 68th Avenue South, Kent, Washington 98032

(Received 2 March 1983 and in revised form 14 November 1983)

The interactions of compliant coatings with laminar, transitional and turbulent boundary layers are investigated. A 2 m long flat plate is towed in the range of speeds of 20–140 cm/s in an 18 m water channel using a carriage riding on an oil film. Isotropic and anistropic compliant coatings are used to cover about 20% of the working Plexiglas surface. The compliant material used is a viscoelastic plastisol gel produced by heating a mixture of polyvinyl chloride resin, a plasticizer and a stabilizer, and allowing them to gel. The shear modulus of rigidity of the plastisol was varied by changing the percentage of PVC in the mix. Anisotropy is introduced by placing the plastisol on a rubber surface having longitudinal grooves scaled with the low-speed streaks in the turbulent boundary layer. The most pronounced effect of the surface compliance in a turbulent boundary layer is a hydroelastic instability in the form of a spanwise wave structure on the compliant surface. The compliant-surface deformation was measured using a novel remote optical technique. The onset speed of the hydroelastic instability waves depends on the thickness and the modulus of rigidity of the plastisol. Their wavelength, wave speed and amplitude are found to depend on these plastisol parameters as well as on the towing speed. In a laminar boundary layer with freestream speeds of over twice the corresponding onset velocity for the turbulent case, no similar instability is observed.

1. Introduction

The motion of fluid over a surface that complies to the flow offers the potential for a rich variety of fluid/surface interactions. Surface stresses induced by the fluid may cause movement in the compliant surface, which in turn can result in significant changes in the basic flow properties. For example, the motion of air over a water surface creates an air/surface interaction crucial to the exchange of momentum as well as the transport of heat, moisture and various chemicals. In the past several decades, some attention has been focused on air or water flow over compliant solids. If the surface can be designed to comply to the flow, then the properties of the flow may be different from those on a rigid plate. In particular, the dynamic processes occurring in a turbulent boundary layer, e.g. bursts and low-speed streaks, may be affected, as well as scalar and momentum transport. Much of the past work has addressed the possibility of designing the properties of the compliant surface in order to reduce the momentum transport and hence the drag.

The idea of using compliant coatings for drag reduction was suggested by Kramer

† Permanent address: Department of Aerospace Engineering, University of Southern California, Los Angeles, CA 90007.

‡ Present address: Department of Mechanical Engineering, University of Washington, Seattle, WA 98105.

(1957) based on observations of dolphins swimming in water. It was suggested that the stability and transitional characteristics of a boundary layer may be influenced by coupling it hydroelastically to a compliant coating. In the early 1960s, Kramer (e.g. 1962) reported substantial drag reduction for towed underwater bodies covered with compliant coating. He hypothesized that, by tuning the elastic wall damping to a frequency near that of the most-unstable Tollmien–Schlichting wave, it would be possible to dissipate the instability waves partially, thus delaying the transition to turbulence. Kramer's tests were performed by towing a test model behind a motor boat in Long Beach Harbor. Unfortunately, many attempts by other investigators to repeat Kramer's experiments under more-controlled conditions failed to yield similar conclusions (e.g. Puryear's (1962) experiment in a towing tank).

Theoretical work by Benjamin (1960); Betchov (1960); Landahl (1962) and Kaplan (1964) indicated that transition would be slightly delayed for certain compliant surfaces. However, the theoretically predicted successful coatings had specific characteristics that would be extremely difficult to match in practice. It is important to note that almost all this early work addressed the delay of transition and ignored the potential for reducing turbulence skin friction with compliant coatings.

During the mid-1960s, Benjamin (1964) explored the possibility that a compliant coating might also affect the skin-friction drag in a fully developed turbulent boundary layer. Blick and his coworkers at the University of Oklahoma (e.g. Smith & Blick 1969) experimentally demonstrated significant reduction in turbulence skin friction for compliant surfaces in air. Subsequent tests by Lissaman & Harris (1969), who attempted to substantiate Blick's conclusions, yielded only extremely modest gains. Recently, McMichael, Klebanoff & Moore (1980) have demonstrated that the apparent reduction in turbulence skin friction in the University of Oklahoma's experiments could be a consequence of experimental deficiences coupled with improper interpretation of the data.

During the 1970s various compliant materials were tested in water, but in *no* case was a statistically significant reduction of drag measured. Bushnell, Hefner & Ash (1977), in summarizing the work at the NASA Langley Research Center and the general status of compliant-surface drag reduction, stated that, while it was possible to increase the transition Reynolds number by perhaps a factor of two, there was no definitive reduction of drag for *turbulent* flows in air. They also stated that drag reduction in turbulent flows in water may be probable because surfaces can be built with impedances more closely matched to those of the fluid.

McMichael *et al.* (1980) stated that no turbulent-boundary-layer experiments have conclusively found any drag reduction using compliant surfaces. On the other hand, conditions have been identified in which hydrodynamic drag is increased due to flow-induced deformations in the compliant surface. Boggs & Hahn (1962) were the first to point to the existence of a large-amplitude spanwise wave structure at a compliant-surface–fluid interface due to the fluid motion. These 'static-divergence' waves appeared after the freestream exceeded an onset velocity threshold. Theoretical work by Weaver & Unny (1970, 1973) confirmed the existence of this hydroelastic instability. In a series of experiments, Hansen & Hunston (1974*a*, *b*, 1976, 1983) and Hansen *et al.* (1980*a*, *b*) established several quantitative characteristics of the static-divergence waves, such as the conditions for their initiation, propagation speed and influence on hydrodynamic drag.

During the last two decades, significant advances have been made in understanding the underlying processes involved in turbulent boundary layers. These advances have generally resulted from visualization studies which have identified coherent eddy

structures (e.g. Kline *et al.* 1967; Corino & Brodkey 1969; Falco 1977) and detailed probe measurements directed at the visually observed features (e.g. Kovasznay, Kibens & Blackwelder 1970; Willmarth & Lu 1972; Blackwelder & Kaplan 1976). These studies have shown that near the solid surface the fluid is organized into elongated streamwise regions of high- and low-speed fluid, alternating in the spanwise direction and appearing randomly in space and time. The low-speed regions, observed in flow-visualization experiments as areas of tracer accumulation, are referred to as low-speed streaks. Directly above the low-speed regions, inflectional velocity profiles develop and appear to produce an inviscid instability in the buffer region of the boundary layer. Shortly thereafter, a burst occurs characterized by a significant amount of low-speed fluid being ejected from the wall region and resulting in a very large local Reynolds stress. It appears plausible that a successful compliant surface would somehow have to disrupt this bursting process.

Bushnell *et al.* (1977) hypothesized that a successful compliant coating would modulate the preburst flow in the turbulent boundary layer by providing a pressure field that would tend to inhibit the burst formation. This would result in a reduced number of bursts occurring per unit time and consequently a lower skin-friction drag. Orszag (1979) assumed this conceptual model and performed numerical calculations of the turbulent boundary layer to explore the effects of compliant surfaces. His results, although preliminary, indicated that turbulence drag reduction might be possible for certain classes of materials. He concluded that relatively short wavelengths within a compliant wall may have an appreciable effect in stabilizing the boundary layer to further bursts.

The current state of experimental and theoretical research on compliant coating is inconclusive, confusing, and inadequate. Fischer & Ash (1974) attributed the confusion to the failure of many investigators to identify and isolate the parameters that contributed to drag reduction in compliant coating studies. No experiments to date have conclusively demonstrated reproducive turbulence skin-friction reduction using compliant surfaces. On the theoretical side, a qualitative picture of the basic eddy structures within a turbulent boundary layer on a flat plate has not yet been completed. Thus, adequate models do not exist to treat turbulence skin-friction modification and hence cannot be used as a guide in choosing successful compliant surfaces.

The objectives of the present investigation were to examine the interaction of compliant surfaces with boundary-layer flows, without immediate regard to whether drag reduction was achieved. Thus the goals were to obtain some baseline data on the interaction between the fluid and solid which may be useful toward modelling this complicated physical phenomenon. Flow-visualization and probe-measurement experiments were conducted in a towing tank using a flat-plate geometry. The effects of the compliant coatings on laminar, transitional and turbulent boundary layers were determined for a range of speeds above and below the onset speed for static-divergence waves. Definitive data on these waves were acquired using a novel remote optical technique.

2. Experimental equipment and procedure

2.1. *Test facility*

The 18 m long, 1.2 m wide and 0.9 m deep towing tank and associated equipment have been described by Gad-el-Hak, Blackwelder & Riley (1981). The flat plate was rigidly mounted under a carriage that rides on two tracks mounted on top of the towing tank. During towing, the carriage was supported by an oil film which ensured

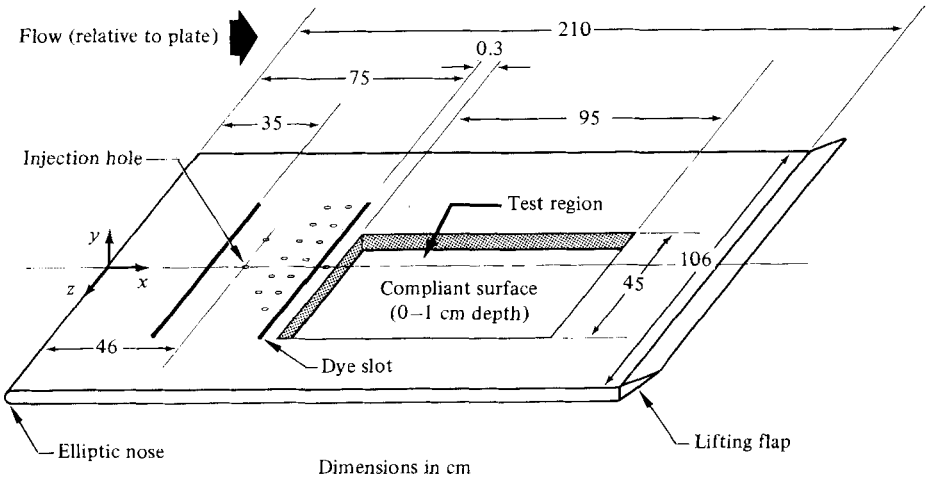

FIGURE 1. Schematic of the flat plate.

a vibrationless tow, having an equivalent freestream turbulence of about 0.1 %. The carriage was towed by two cables driven through a reduction gear by a 1.5 h.p. Boston Ratiotrol motor. The towing speed was regulated within an accuracy of 0.1 %. The system was able to achieve towing speeds between 20 and 140 cm/s for the present study. The flat plate used in the present experiment is sketched in figure 1. An aluminium frame provided a flat bed for the Plexiglas working surface. The gaps in the aluminium frame were filled with lightweight styrofoam, and the frame was painted with marine enamel to prevent corrosion. The whole structure was buoyant in water and was flat to within 0.2 mm. Care was taken to avoid leading-edge separation and premature transition by having an elliptic leading edge and an adjustable lifting flap at the trailing edge. The flap was adjusted so that the stagnation line near the leading edge was located on the working surface. The working surface was smooth and was 210 cm long and 106 cm wide. A 45 cm by 95 cm well was built into the working surface for placing compliant materials of up to 1 cm in thickness.

A laminar boundary layer was obtained over the entire working surface for towing speeds of 20–80 cm/s. Trips were used to generate a fully developed turbulent boundary layer, and a single roughness element was used to generate a turbulent wedge embedded in the laminar boundary layer. The trips were brass cylinders with 0.32 cm diameter and 0.25 cm height placed 20 cm behind the leading edge, and having their axes perpendicular to the flat plate. To generate turbulent spots, a 0.4 mm diameter injection hole located at $x = 46$ cm on the working surface provided a small squirt of water into the laminar flow. The injection was controlled with a constant-head tank and a solenoid valve.

2.2. *Compliant material*

The compliant material used in the present investigation was a plastisol gel made by heating to 160 °C a mixture of polyvinyl chloride resin (PVC), dioctyl phthalate (plasticizer), and dibutyl tin maleate (stabilizer). The mixture was poured in a heated aluminium pan and allowed to cool gradually to complete the gelation process. The pan was then placed inside the well in the working surface and its height was adjusted from the bottom to insure a flush smooth surface.

Whenever a new coating was poured, a $0.6 \times 10 \times 10$ cm sample was produced from the same mixture to measure the modulus of rigidity G. The modulus value was quite sensitive to small differences in the mixing process at the low PVC concentrations used. For example, a nominal 3% PVC mixture would have moduli differing by 50–100%. The shear modulus of rigidity was measured with an automated strain gauge/LVDT device which subjected the sample to a prescribed shear force and the displacement was measured. The force-versus-displacement curve was always linear in spite of the fact that displacements of approximately 50% of the thickness were used. Extremely rapid loading or unloading yielded higher values of G and indicated the 3% PVC solids had a relaxation time constant of approximately one second. Since the elastic properties of the material change considerably during gelling, the compliant surface and the sample were allowed to sit in air for one day before testing. The gelling process seemed independent of whether the material was in air or water. Whenever data were taken with the coating, the shear modulus was simultaneously measured on the sample. The repeatability of the modulus measurement was approximately 20% on samples from the same batch.

The modulus of rigidity G of the plastisol was varied in the range 50–125000 dyn/cm^2 by changing the percentage of PVC from 3% to 25% in the mixture. The stabilizer was always 10% of the PVC by weight. The specific gravity of the plastisol was approximately unity and had a weak dependence upon the age of the material and the percentage of PVC in the gel.

2.3. *Flow visualization*

The turbulent regions were made visible by novel techniques which utilized fluorescent dye, i.e. dye that is visible only when excited by a strong light source of the appropriate wavelength (Gad-el-Hak *et al.* 1981). This provided an extra degree of freedom in observing the flow because both the dye and light location could be controlled within the limitations of the experimental apparatus. In order to generate a sheet of light that could be projected at any desired orientation, a 5 W argon laser (Spectra Physics Model 164) was used with a mirror mounted on an optical scanner having a 720 Hz natural frequency (General Scanning Inc.) driven by a sine-wave signal generator of the desired frequency. The frequency of the sine wave was usually set equal to the inverse of the shutter speed of the camera. The light sheets were approximately 1 mm thick, which was sufficient to resolve the large structure within the turbulent regions.

Different methods of dye injection were employed. Dye sheets were seeped into the boundary layer through two spanwise slots 0.15 mm wide. The first was 30 cm long and was located 35 cm downstream of the leading edge. The second slot was 50 cm long and was located 75 cm downstream of the leading edge. The slots were milled at a 45° angle inclined toward the trailing edge to minimize the flow disturbance.

2.4. *Hot-film probes and pattern-recognition techniques*

Miniature boundary-layer hot-film probes (TSI Model 1260) were used in the present investigation to measure the longitudinal mean and fluctuating velocities. The probe diameters were 0.025 mm and their sensing lengths were 0.25 mm. Conventional statistical quantities, such as the mean and the root mean square, were computed from the velocity signals.

A new technique, which utilizes the streamwise velocity signals from three hot-film probes, was developed to detect low-speed streaks. The probes were located at $y^+ = 10$ at the same streamwise position with a spanwise separation of approximately 20 ν/u_τ.

Thus the total array spanned $40\,\nu/u_\tau$, which is approximately half the average low-speed streak spacing. A pattern recognition algorithm identified a low-speed region whenever all three signals were less than the local mean velocity by one-half an r.m.s. value and the velocity measured by the middle probe was less than the velocity on either side. The beginning and end of each low-speed region could thus be identified, and the streaks' average length and frequency computed.

To test this algorithm, experiments were first carried out using a rake of twelve velocity probes located at $y^+ = 10$, but having a significantly broader spanwise extent. Low-speed streaks were readily identified using the isovelocity contours computed from the rake's output, and their spacing was in reasonable agreement with results obtained from visualization experiments conducted under similar conditions. The results of the algorithm were compared with the low-speed streaks obtained from the rake. The comparison showed that the detected algorithm picked out the streaks exceedingly well, and that the streaks meander in the spanwise direction so that often a single streak crosses the probes two or more times, resulting in multiple detections.

The second pattern-recognition algorithm employed was a burst detection scheme using the variable-interval time-averaging (VITA) technique developed by Blackwelder & Kaplan (1976). A single hot-film probe located at $y^+ = 20$ was used for burst detection. Identical detection parameters were used for both rigid and compliant surfaces. The program counted the number of bursts that occur near the wall and recorded their intensities.

2.5. *Measurements of compliant-surface deformation*

The vertical displacement of the compliant surface was measured by a remote technique† which employed a Reticon camera (Model LC600V) equipped with an array of 256 photodiodes spaced 25 μm centre to centre. A vertical beam of an argon laser having a diameter of 1 mm produced a bright spot where it intersected the compliant surface, which contained minute amounts of Rhodamine-6G fluorescent dye. The camera and the laser beam were fixed in space, and the flat plate was towed at a known speed. The axis of the photodiode array was aligned with the vertical laser beam, and the bright spot on the compliant surface was imaged onto the photodiode array via a set of lenses and extension tubes. Thus the digital output resulting from the continuous scanning of the photodiode array output indicated the vertical displacement of the compliant surface along a line parallel to the flow. Calibration of the device was accomplished by vertically traversing the Reticon camera while the plate was fixed. The system had a frequency response of 1 kHz, and resolved vertical displacements as low as 0.03 mm. The surface deformations were also recorded using a ciné camera.

3. Discussion of the compliant material

Both static and dynamic tests were made to determine the mechanical properties of the coatings. For the range of stresses applied (from 0 to 1000 dyn/cm^2, which is broader than the range of stresses expected to be induced by the flow), and for the percentages of PVC used, the static tests indicated that the relation between the applied shear stress and the resulting shear strain was linear. For the dynamic tests, a shear stress was applied until the system came into equilibrium, and the stress was suddenly released. The value of the subsequent strain was observed using an LVDT

† The device is called a 'laser displacement gauge', and was developed for wind-wave measurements by Liu, Katsaros & Weissman (1982).

and a Nicolet digital oscilloscope (Model 4094). The observed time history indicated that the plastisol was a viscoelastic solid of the generalized Kelvin type (Jaeger & Cook 1976). The time constant of the plastisol decreased as the percentage of PVC in the mix increased. For PVC percentages used in the experiments, a typical value for the relaxation time was about 1 s, which was larger than the timescales in the turbulent boundary layer.

Some understanding of how a compliant surface will respond to the flow above it can be obtained by examining the free-surface waves of the coating. As pointed out by Rayleigh (1887), the surface waves can be modelled as a linear combination of waves having displacements perpendicular or parallel to the propagation direction. These are called transverse and longitudinal displacement waves respectively. Assuming that the coating is a linear elastic solid, both wave systems satisfy the wave equation (see e.g. Landau & Liftshitz 1970):

$$\frac{\partial^2}{\partial t^2}\eta - c^2\left(\frac{\partial^2}{\partial x^2}+\frac{\partial^2}{\partial y^2}\right)\eta = 0, \tag{1}$$

where η is a component of the displacement vector, and x and y are coordinates parallel and normal to the undisturbed surface. The propagation velocities are $x = c_t = (G/\rho_s)^{\frac{1}{2}}$ for the transverse waves, and $c = c_l = [(\lambda+2G)/\rho_s]^{\frac{1}{2}}$ for the longitudinal waves, where G and λ are elastic constants and ρ_s is the density of the solid.

The free-surface wave dispersion relationship is obtained by assuming that the wave solutions have exponential dependence on distance measured normal to the surface y and have harmonic dependence on distance measured along the surface x and on time t:

$$\xi = (A\sinh\alpha y + B\cosh\alpha y)\,\mathrm{e}^{\mathrm{i}(kx-\omega t)}, \tag{2a}$$

$$\eta = (C\sinh\alpha y + D\cosh\alpha y)\,\mathrm{e}^{\mathrm{i}(kx-\omega t)}, \tag{2b}$$

where ξ is the displacement in the x-direction and η is the corresponding displacement in the y-direction. Note that for real α the waves decay exponentially with depth, whereas for imaginary α they oscillate with depth. Substituting these solutions into the wave equation (1), and applying the boundary conditions

$$(c_l^2-2c_t^2)\frac{\partial\xi}{\partial x}+c_l^2\frac{\partial\eta}{\partial y} = 0 \quad \text{no normal stress at the surface } (y=0), \tag{3a}$$

$$\frac{\partial\xi}{\partial y}+\frac{\partial\eta}{\partial x} = 0 \quad \text{no tangential stress at the surface } (y=0), \tag{3b}$$

$$\xi = 0, \quad \eta = 0 \quad \text{no displacement at the bottom } (y=-d) \tag{3c}$$

results in the following dispersion relationship:

$$M(\zeta) \equiv 4\frac{\alpha_t\alpha_l}{k^2}\left(2-\zeta^2\right)-\frac{\alpha_t\alpha_l}{k^2}\left[4+\left(2-\zeta^2\right)^2\right]\cosh\alpha_t d\cosh\alpha_l d$$
$$+\left[4\frac{\alpha_t^2\alpha_l^2}{k^4}+\left(2-\zeta^2\right)^2\right]\sinh\alpha_t d\sinh\alpha_l d = 0, \tag{4}$$

$$\alpha_t = k(1-\zeta^2)^{\frac{1}{2}}, \quad \alpha_l = k(1-\zeta^2R^2)^{\frac{1}{2}},$$

where $R = c_t/c_l$ is the ratio of the transverse to the longitudinal wave speed, k is the longitudinal wavenumber and $\zeta = c_p/c_t$ is the ratio of the surface-wave speed to the transverse-wave speed.

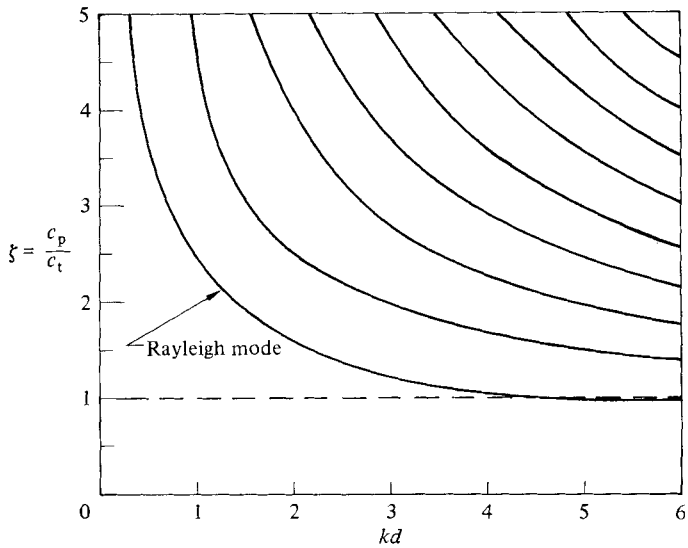

FIGURE 2. Solutions of the dispersion equation.

Plots of dispersion curves resulting from (4) are given in figure 2 for the case $R = 0$, which is close to the experimental conditions. Note that only one solution has a surface-wave speed below $c_t (\zeta < 1)$. This solution approaches its asymptote $\zeta = 0.956$ for large kd, which is the value of Rayleigh's infinite half-layer solution. Also note that, as ζ increases for a given kd, the possibility exists for a richer range of interactions of the coating and the flow. Typical values for kd in the experiments, with wavelength $2\pi/k$ taken as the boundary-layer thickness, are in the range of about 1–5. Figure 2 indicates that compliant surface/flow interactions may not be expected for flow speeds, much below c_t, and the best opportunity for interactions will be for flow speeds well above c_t. Unfortunately, as will be shown in §4.2, static-divergence waves appear for freestream speeds somewhat above c_t, thus limiting the opportunities for interaction without the contamination of these waves present.

The above dispersion relation does not reflect the effect of the fluid motion on the compliant surface. The analysis can be extended to include the surface stress induced by a fluid moving over the coating. Some general aspects of this case have been addressed by, among others, Benjamin (1960, 1963), Landahl (1962) and Kaplan (1964). Benjamin and Landahl have conducted stability analyses and have established that three types of instability waves may exist. The first type, labelled class A, is an instability which is destabilized by the addition of dissipation in the system. Duncan, Waxman & Tulin (1982) have suggested that pressure phase lags transfer energy from the coating to the flow which stabilizes these waves. Static-divergence waves appear to be a member of this class. The second type, class B, is stabilized by damping and destabilized by pressure effects; and the third, class C, corresponds to a Kelvin–Helmholtz type of instability, where the waves grow or decay primarily through reversible processes. Kaplan (1964) has computed solutions for specific cases.

Assuming that the surface stress of primary importance due to the fluid is pressure, the effect of the fluid motion on the compliant surface can be simply modelled by considering the basic flow over the coating as inviscid and unsheared, and hence using potential-flow theory to determine the surface pressure in terms of the surface displacement. Duncan *et al.* (1982) have recently explored the dispersion relation for a

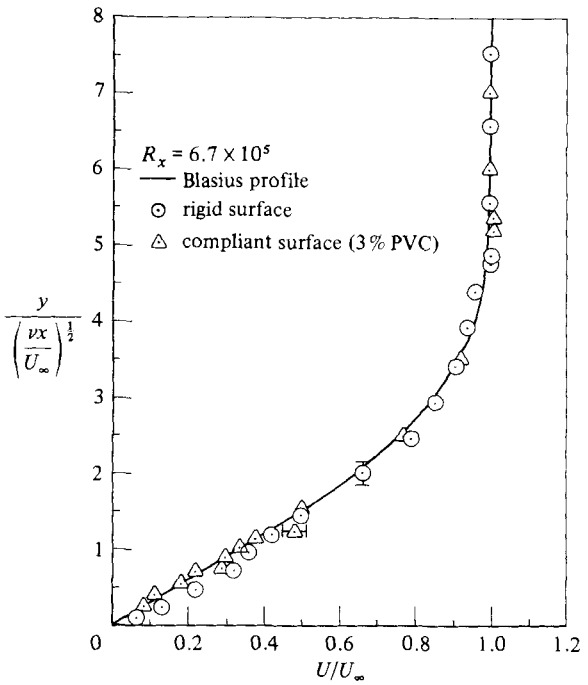

FIGURE 3. Laminar-boundary-layer profiles.

one-layered viscoelastic solid. The pressure applied at the surface was a generalization of the potential-flow solution to include arbitrary amplitude reduction and phase shift. Some of the implications of their analysis on the present experimental results will be discussed in §4.

4. Experimental results

4.1. *Hot-film-probe measurements in absence of static-divergence waves*

The compliant coatings were initially tested to determine their effect on laminar boundary layers. Several boundary-layer traverses were taken on different coatings having a shear modulus of rigidity $150 < G < 5000$ dyn/cm^2. The boundary-layer profiles were all found to agree with the Blasius solution within the experimental accuracy, as seen in figure 3.

The mean and r.m.s. streamwise velocity profiles were measured in turbulent boundary layers at Reynolds numbers of $1.5 \times 10^5 < U_\infty x/\nu < 2.8 \times 10^6$ ($400 < U_\infty \delta^*/\nu < 6000$) on several different surfaces. Typical results are seen in figure 4. The friction velocity used for normalizing the data from both rigid and compliant surfaces was computed using Clauser's (1956) method. The mean-velocity profiles always had well-defined logarithmic and wake regions, and agreed with the solid-surface data as long as static-divergence waves were not present. Similarly, the r.m.s. values agreed well with the rigid-surface data. In addition, the bursting frequency remained constant at $f^+ = 0.004$, and no significant differences were observed in the number or the length of recorded streaks. Thus, as long as the static-divergence waves were absent, the velocity measurements suggested that a laminar or turbulent boundary layer over the compliant surface did not differ from that on a rigid surface.

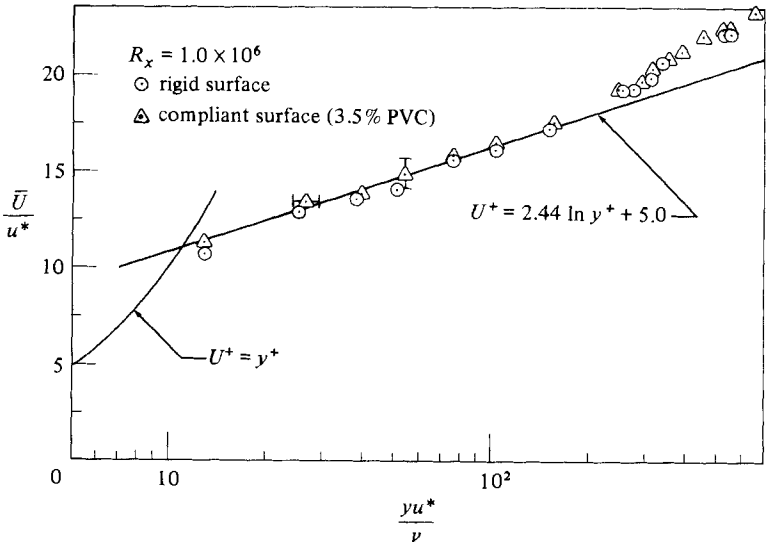

FIGURE 4. Turbulent mean-velocity profiles.

However, as discussed in §4.3, the presence of static-divergence waves significantly altered the structure of the turbulent boundary layer.

4.2. *Onset of static-divergence waves*

One of the principal results of the present work has been the definitive data acquired on static-divergence waves. The slowest-travelling free-wave speed on the surface of a solid is given approximately by the transverse-wave speed

$$c_t = (G/\rho_s)^{\frac{1}{2}},$$

where G is the shear modulus of rigidity and ρ_s is the density of the solid. Whenever the freestream velocity U_∞ above the turbulent boundary layer became sufficiently large that $U_\infty/(G/\rho_s)^{\frac{1}{2}}$ exceeded a critical value, which depends on the thickness d of the coating, static-divergence waves appeared on the solid's surface. A typical example of these waves is shown in figure 5. The 3% PVC plastisol coating had a thickness of $d = 0.71$ cm and the flow speed was $U_\infty = 40$ cm/s, yielding $U_\infty/(G/\rho_s)^{\frac{1}{2}} = 6.3$. The waves appear to have a characteristic wavelength and are approximately two-dimensional. A ciné film of this and other runs is available on request (Flow Research Film 53).

The onset speed of static-divergence waves for different moduli of rigidity and thicknesses was determined from visual observation of the compliant surface. The results are shown in figure 6. The ratio $U_{\text{onset}}/(G/\rho_s)^{\frac{1}{2}}$ decreases as the compliant-coating thickness increases. In other words, thick surfaces are more susceptible to this hydroelastic instability than thin ones. This result apparently has not been reported in the literature before. For large thicknesses, the non-dimensional onset speed tends towards the value 3, reported by Hansen & Hunston (1974*a*).

The onset of static-divergence waves present a dilemma, because, if there is to be a rich fluid/solid interaction, the convection velocities in the fluid must lie within the range of the propagation velocities in the solid. On the other hand, when the two velocities are comparable, static-divergence waves occur. Since these waves are the

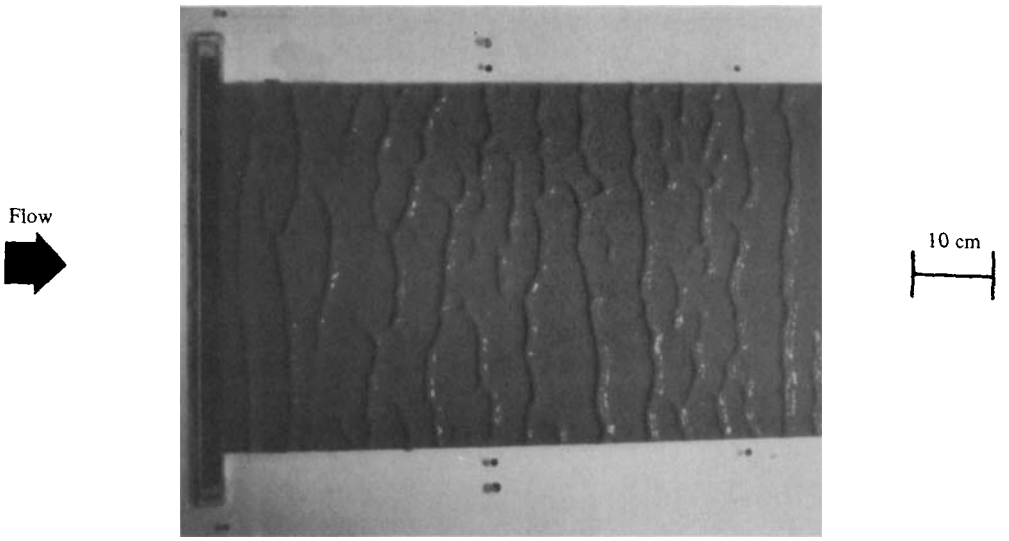

FIGURE 5. Static-divergence waves under a turbulent boundary layer. This plan view shows the coating in the 45 × 95 cm well illustrated in figure 1. $U_\infty = 40$ cm/s, $U_\infty/(G/\rho_s)^{\frac{1}{3}} = 6.3$, $d = 0.71$ cm.

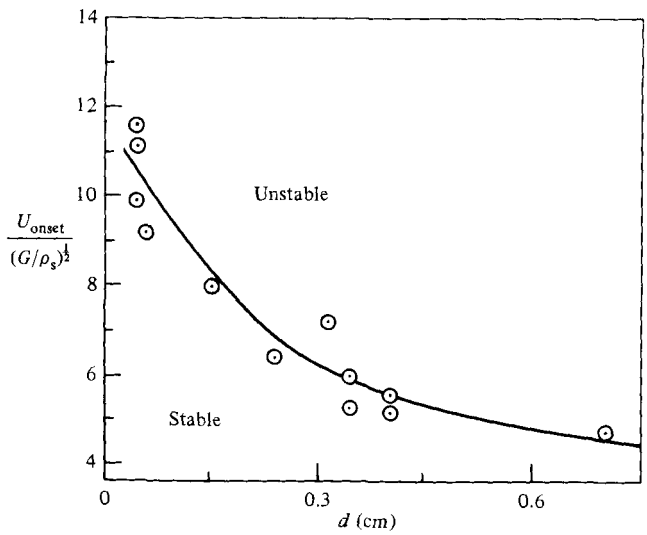

FIGURE 6. Onset-speed dependence on thickness. This line is a least-squares fit of the data.

result of a strong interaction between the fluid and the solid, an investigation of this interaction was deemed useful toward understanding the physics of the energy transfer across the fluid/solid interface.

4.3. *Flow-visualization results*

Flow-visualization experiments were carried out for a broad range of compliant-coating parameters, and for laminar, transitional and turbulent boundary layers. In the case of turbulent boundary layers, static-divergence waves were observed whenever the towing speed was above the critical onset speed, which depended on the depth of the

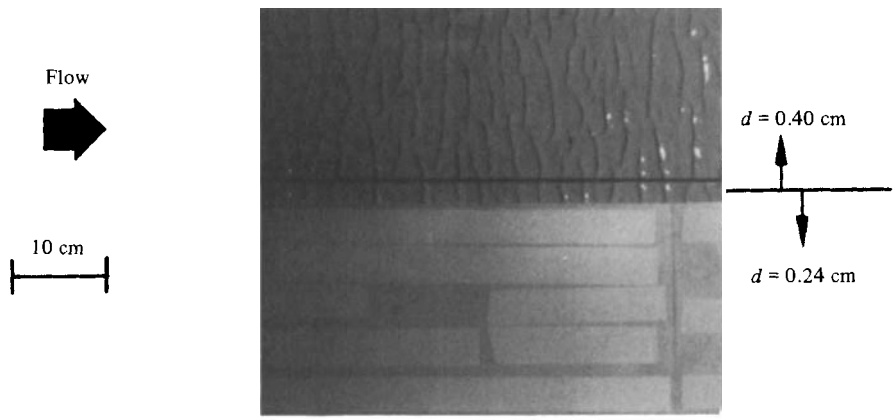

(a)

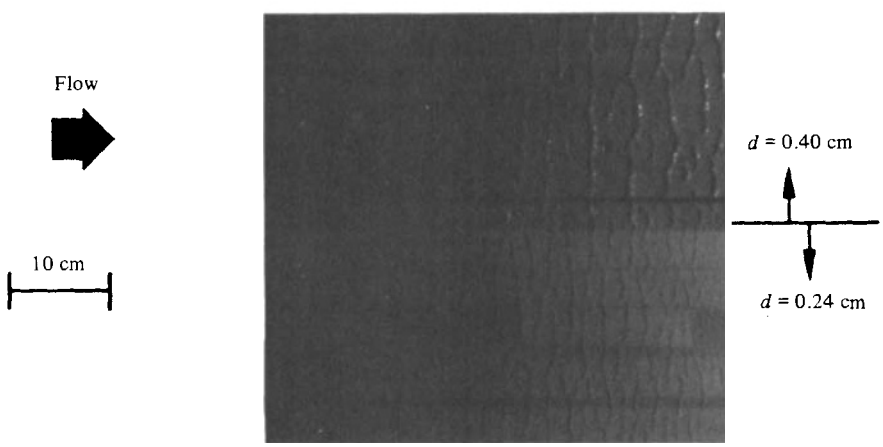

(b)

FIGURE 7. Effect of thickness on static-divergence waves; $d_1 = 0.40$ cm, $d_2 = 0.24$ cm: (a) $U_\infty = 60$ cm/s, $U_\infty/(G/\rho_s)^{\frac{1}{3}} = 6.5$; (b) 80 cm/s, 8.7.

coating as shown in figure 6. An example of this depth dependence is illustrated in the two photographs shown in figure 7. The flow is from left to right, and the upper half of the coating in each photograph had a depth of 0.4 cm and the lower half had a depth of 0.24 cm. The depth change was attained by placing a false bottom in the lower half of the aluminium pan, so that both compliant surfaces were flush with the flat plate. In figure 7 (*a*) the velocity $U_\infty = 60$ cm/s ($U_\infty/(G/\rho_s)^{\frac{1}{3}} = 6.5$) exceeded the critical onset speed reported by Hansen & Hunston (1974*a*). The static-divergence waves appear over the thicker surface; however, they do not exist on the lower, thinner surface. In figure 7 (*b*) $U_\infty = 80$ cm/s ($U_\infty/(G/\rho_s)^{\frac{1}{3}} = 8.7$), and waves appear on both the thick and the thin compliant coatings. The flow speed is now above the onset speed for both the top and bottom layers. The wavelength of the static-divergence

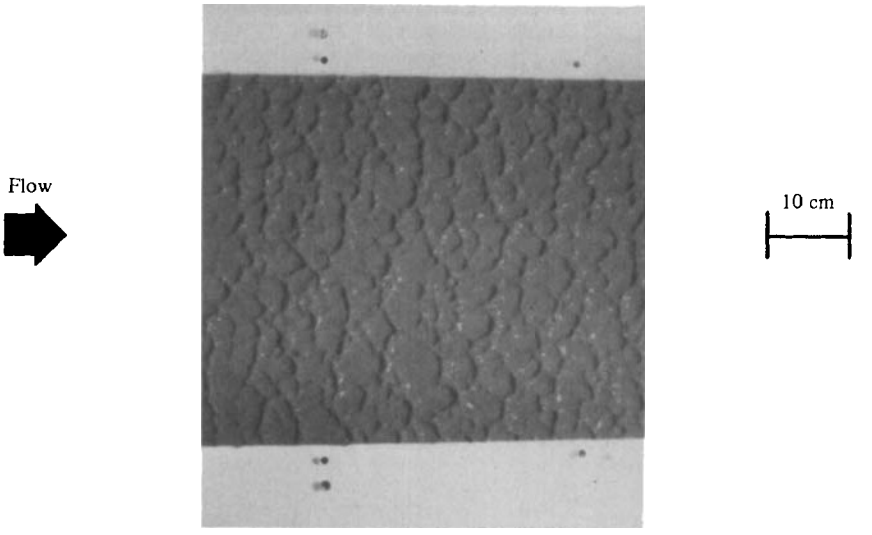

FIGURE 8. Three-dimensional effects at high flow speed; $U_\infty = 121$ cm/s, $U_\infty/(G/\rho_s)^{\frac{1}{2}} = 19.2$, $d = 0.71$.

waves also was found to depend upon the layer depth. As seen in figure 7(*b*), the wavelength is greater on the thicker coating than on the thinner one.

No waves of types I and II reported by Hansen *et al.* (1980*a*) were observed explicitly in the present visualization runs. These waves were apparently due to small discontinuities between the coating and the rigid surface in the experiment of Hansen *et al.* Considerable effort was expended to minimize such discontinuities in the present experiment, which possibly explains why these waves were not observed.

At velocities near the onset speed, the static-divergence waves were nearly two-dimensional, as seen in figure 5. As the velocity was increased, it seemed that small non-uniformities in the amplitude along the crests were magnified. Other crescent-shape waves can be seen forming downstream of these irregularities, thus reducing the average wavelength. As the velocity increased further, the three-dimensional effects became stronger. As seen in figure 8 for $U_\infty/(G/\rho_s)^{\frac{1}{2}} = 19.2$, the wave pattern is much more three-dimensional that that shown in figure 5. Although the three-dimensional disturbances began with smaller amplitudes, they rapidly grew to amplitudes comparable to the existing waves. In addition, the phase speed of the new waves was the same as that of the existing ones. Hansen & Hunston (1983) also observed that the waves became more complex with increasing velocity. It is not clear whether the appearance of the three-dimensional waves at higher flow speeds is a further manifestation of the static-divergence waves, or that other kind of surface instabilities are becoming apparent.

Whenever the static-divergence waves appeared, they had an amplitude comparable to the depth of the coating and presented an extremely rough surface and a severe distortion to the flowfield. To investigate the effects of the waves on the turbulent boundary layer, the large eddies were visualized using fluorescein dye injected from a spanwise slot at $x = 75$ cm. The dye was illuminated with a sheet of laser light in the (x, y)-plane. The compliant surface had no effect on the large eddies as long as the static-divergence waves were absent. However, the presence of these waves dramatically changed the large-eddy structure. Figure 9 shows two photographs of

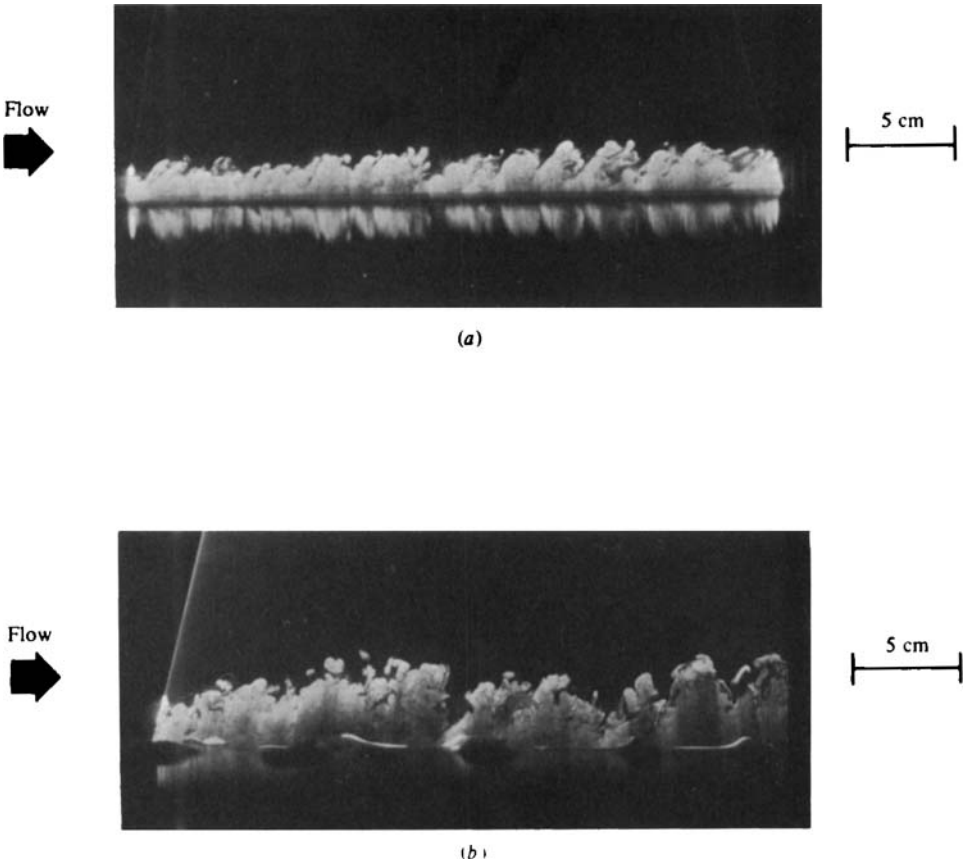

FIGURE 9. Large-eddy structure in a turbulent boundary layer; $U_\infty = 50$ cm/s, $x \approx 120$ cm: (*a*) solid surface; (*b*) compliant surface; $U_\infty/(G/\rho_s)^{\frac{1}{3}} = 8$, $d = 0.71$ cm.

the large eddies at $x \simeq 120$ cm and $U_\infty = 50$ cm/s. The upper picture presents a turbulent boundary layer over a rigid wall and the lower one shows the eddies over a compliant wall such that $U_\infty/(G/\rho_s)^{\frac{1}{3}} = 8$. The peaks of static-divergence waves in the lower photograph are quite sharp and their valleys are shallow and broad. The presence of the waves caused a 100% increase in the average eddy height. Since the static-divergence waves were so dynamically significant in the turbulent boundary layers, further data was taken using the Reticon camera to clarify their properties (§4.4).

In laminar-boundary-layer experiments, static-divergence waves were never observed under any condition. Experiments were performed at speeds up to twice the onset speed in the turbulent case without attaining static divergence. An illustration of this is given in figure 10 using a single roughness element located at $x = 75$ cm to produce a turbulent wedge in an otherwise-laminar boundary layer. The flow speed was chosen to be above the critical onset speed for this case. Dyelines emanated from holes spaced 1 cm apart in the spanwise direction at $x = 65$ cm. In the laminar regions the dyelines were unmixed across the plate length. However, the turbulence in the wedge rapidly mixes and diffuses the dye as shown by Gad-el-Hak *et al.* (1981). Static-divergence waves are readily apparent under the turbulent wedge in figure 10, but do not appear in the laminar regions. In this run the 3% PVC

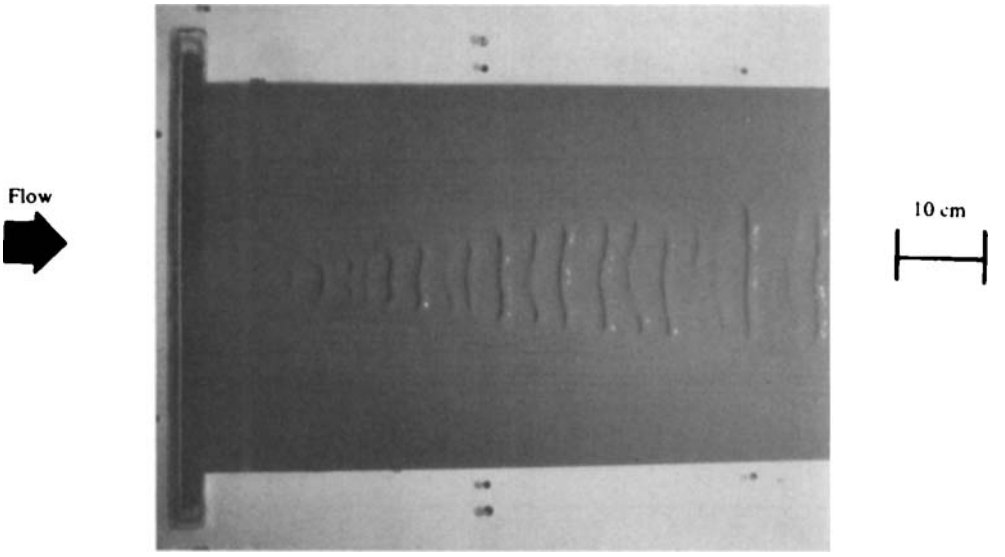

FIGURE 10. Static-divergence waves under a turbulent wedge; $U_\infty = 35$ cm/s, $U_\infty/(G/\rho_s)^{\frac{1}{3}} = 5.2$, $d = 0.71$ cm.

plastisol has a thickness $d = 0.71$ cm and the flow speed was $U_\infty = 35$ cm/s, yielding $U_\infty/(G/\rho_s)^{\frac{1}{3}} = 5.2$. The spanwise growth of the turbulent wedges studied in this investigation were typically $\pm 8°$, indicating that the compliant surface had no effect on their lateral spreading rate.

A related experiment was also carried out with turbulent spots embedded in a laminar boundary layer. The turbulent spots embedded in a Blasius boundary layer were visualized using fluorescein dye seeping from the spanwise slot at $x = 35$ cm and a horizontal sheet of laser light at $y = 0$. In the range of speeds 20–80 cm/s the gross structure of the turbulent spots on the compliant surface was identical with that on a solid surface, in agreement with Hoyt's (1981) results for spots generated on a water table. However, no evidence of subcritical damping as reported by Hoyt was found in the present investigation. The lateral growth rate of the spots and the convection speeds of their leading and trailing edges were the same for both surfaces. The compliant surface became unstable, however, as the turbulent spot was convected over it whenever the towing speed was higher than the onset speed for static-divergence waves. One interesting observation was that the static-divergence waves required that turbulent flow be present for about one second before they could be visually observed. Likewise, after the turbulent production ceased, e.g. after the spot had passed or whenever the plate with a turbulent boundary layer was abruptly halted, the static-divergence waves decayed with a time constant of the order of 1 s. Consequently the waves could not be seen under a turbulent spot until the spot reached a sufficiently large size that its passage time was greater than about one second. Correspondingly the most readily observable waves appeared near the rear of the spot. The relaxation phenomenon appeared to be another manifestation of the viscoelastic nature of the coating.

It is not yet clear why the static-divergence waves are present in the turbulent boundary layer but not in the laminar boundary layer at the same freestream speed. Theoretical models based on potential-flow theory (§3) cannot explain this, since the

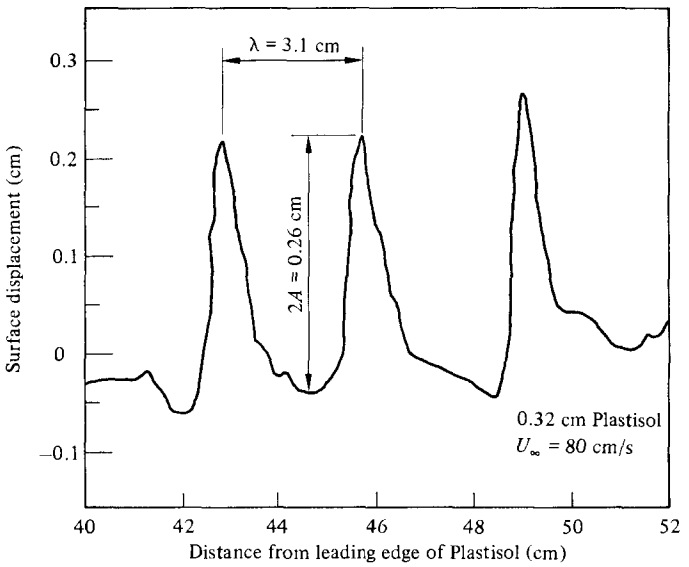

FIGURE 11. Typical surface-wave amplitude measured by the Reticon camera.

influence of the flowfield only comes in through the freestream speed, and hence laminar and turbulent flows are not distinguished. One explanation is that the existence of static-divergence waves depends on the magnitude of the shear stress at the wall. This idea was explored by towing the plate at the highest-possible speed while maintaining a laminar boundary layer (80 cm/s). However, the shear stress was still less than that in the turbulent boundary layer at the onset speed. Thus this point needs to be explored further. An entirely different explanation may be due to the model developed by Duncan *et al.* (1982). This model allows an arbitrary phase shift of the flowfield pressure compared to the phase of the wave, and suggests that the difference may be due to the phase difference of the mean pressure field in the laminar and the turbulent cases.

4.4. *Compliant-surface deformation*

The shape of the static-divergence waves was measured using the Reticon camera. A typical data sample is shown in figure 11. The peak-to-peak amplitude was always comparable to the depth of the coating. Their peaks were always quite sharp and the valleys were shallow and broad. When three-dimensional waves developed at higher velocities, they appeared first as small-amplitude waves in the valleys.

The average wavelength was measured from photographs and ciné films for five different thicknesses of the isotropic coatings. By averaging over several frames the statistical scatter of this random phenomenon was reduced to a standard deviation less than 20%. The average wavelength was also measured for two of the coatings using the output from the Reticon camera and good agreement was obtained with visual measurements. The wavelength has a strong dependence upon the depth of the coating and upon the flow speed as shown in figure 12. For each coating the wavelength increases with U_∞ until a maximum λ_{max} is attained which coincided with the appearance of the three-dimensional wave structure. As the velocity continued to increase, small irregularities along the wave crests seemed to spawn new crescent-shaped waves downstream. As these additional waves appeared over the surface, the

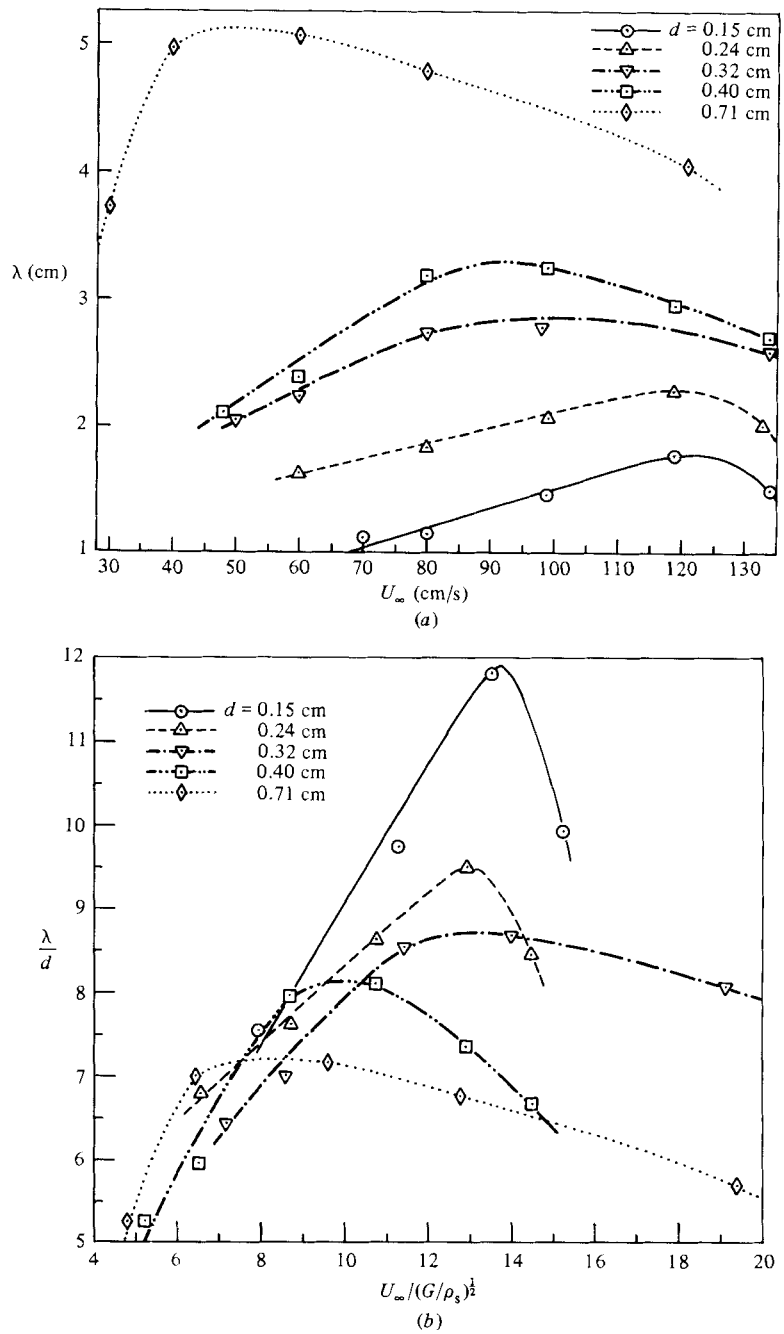

FIGURE 12. Wavelength dependence on thickness and flow speed: (*a*) dimensional plots; (*b*) normalized plots.

average wavelength decreased as seen. Note that the wavelength, at least for low-to-moderate flow speeds, does not scale with the boundary-layer thickness because, as the velocity increases, the spatial scales of the boundary-layer decrease.

The data of figure 12(*a*) are normalized with the thickness d and the transverse wave velocity $(G/\rho_s)^{\frac{1}{2}}$ and replotted in figure 12(*b*). This scaling collapses the data reasonably well for the two-dimensional waves, suggesting that they are highly

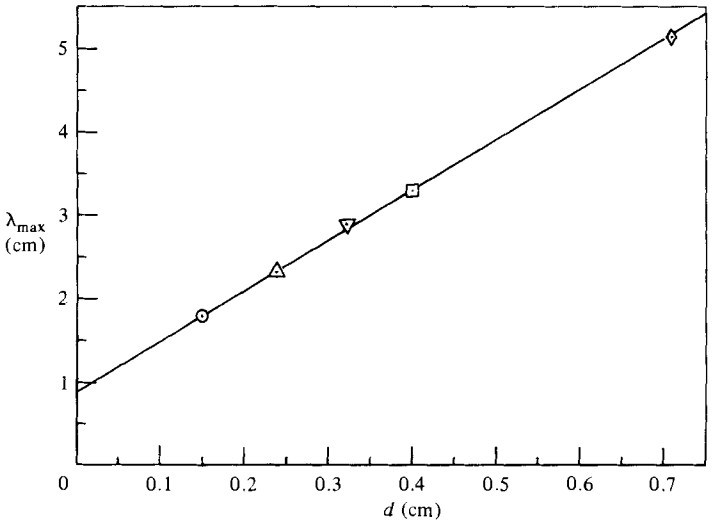

FIGURE 13. Maximum observed wavelength versus compliant-coating thickness.

dependent upon the depth and elastic properties of the coatings. Within the two-dimensional regime a continuous increase in λ/d is observed for all coatings as the velocity increases. Considerable scatter still exists in the three-dimensional wave data as seen.

The difference between the two- and three-dimensional wave structure was quite dramatic as seen by comparing figures 5 and 8. This transition, as denoted by the maximum observed wavelength recorded in figure 12(*a*), is also strongly dependent upon the depth of the coating as shown in figure 13. Although λ_{max} is not directly proportional to the depth, it is curious that it is a linear function of d. The transition to three-dimensional waves occurs at lower velocities as the thickness of the coating increases. Thus it seems that the thicker coatings are more susceptible to the three-dimensional waves.

As their name implies, the static-divergence waves have an extremely low phase speed c_p compared with other characteristic velocities in the fluid and solid. The maximum value of c_p observed in this study was 5% of U_∞. The phase speed c_p depends on the flow speed and the surface thickness as shown in figure 14. Here c_p/U_∞ is plotted against $U_\infty/(G/\rho_s)^{\frac{1}{3}}$ for three different thicknesses, 0.24, 0.4 and 0.71 cm. As the flow speed increases, the phase speed increases, while at a particular flow speed the phase speed increases as the thickness of the coating increases. The dependence on flow speed appears to be given approximately by a power law. A least-squares fit of all the data yields $c_p \sim U^{2.6}$.

The average peak-to-peak amplitude $2A$ was computed from the Reticon camera's output as illustrated in figure 11. The results shown in figure 15 indicate that the peak-to-peak amplitude of the static-divergence waves also depends on the flow speed and increases as the flow speed increases. Since the amplitude data scale with the coating thickness, it appears that the maximum amplitude is limited by the thickness. However, confidence in this result should be tempered by the limited amount of data in the figure.

Another interesting observation was that very few small-amplitude static-divergence waves were ever observed within the constraints of the experiments. No measurable surface deformation were observed as long as the velocity was below the

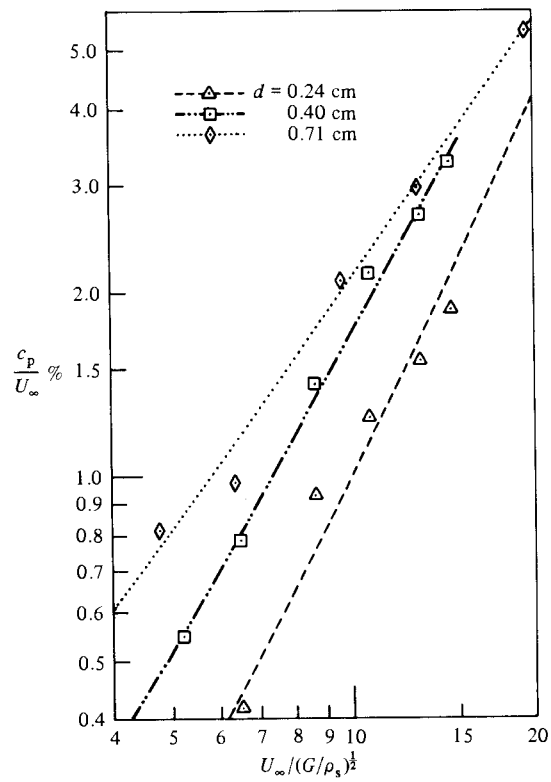

FIGURE 14. Phase speed for static-divergence waves.

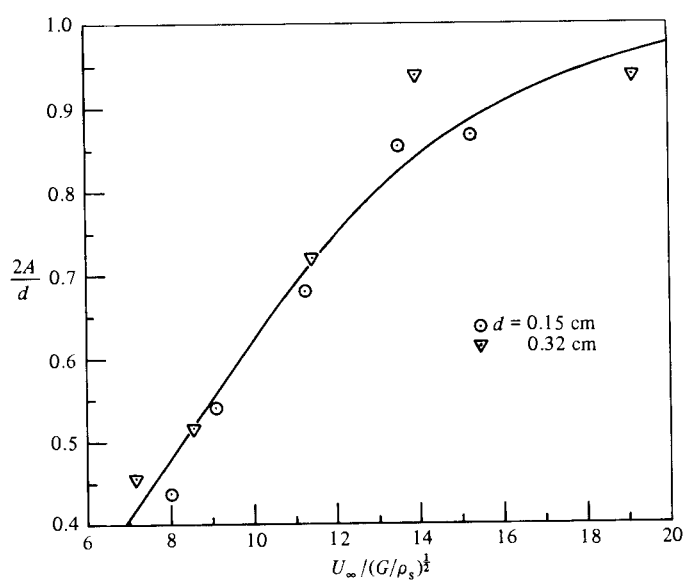

FIGURE 15. Wave-amplitude dependence on thickness and flow speed.

Thickness d (cm)	G (dyn/cm^2)	U_∞ (cm/s)	λ (cm)	$2A$ (cm)	c_p (cm/s)
0.15	77	70	1.13	0.07	—
		80	1.15	0.08	—
		99	1.46	0.10	—
		119	1.77	0.13	—
		134	1.49	0.13	—
0.24	84	60	1.63	—	0.25
		80	1.83	—	0.74
		99	2.07	—	1.23
		119	2.28	—	1.83
		133	2.02	—	2.48
0.32	50	50	2.05	0.15	—
		60	2.24	0.16	—
		80	2.73	0.23	—
		98	2.77	0.30	—
		134	2.58	0.30	—
0.40	84	48	2.11	—	0.26
		60	2.38	—	0.47
		80	3.18	—	1.13
		99	3.24	—	2.13
		119	2.95	—	3.17
		133	2.67	—	4.31
0.71	40	30	3.72	—	0.25
		40	4.97	—	0.39
		60	5.07	—	1.25
		80	4.79	—	2.36
		121	4.05	—	6.46
Nonisotropic compliant surface	71	60	0.55	—	—
		80	0.83	—	—
		89	1.00	0.07	—
		99	1.17	0.07	—
0.05–0.22		110	1.03	0.08	—
		117	0.98	0.06	
		134	0.98	0.05	

TABLE 1. Characteristics of static-divergence waves

threshold; and, immediately above the threshold velocity, waves with amplitude of typically $2A/d = 0.5$ appeared.

The characteristics of the static-divergence waves for different moduli of rigidity and thicknesses are summarized in table 1. In addition to five different isotropic coatings, the table contains some preliminary results of an anisotropic coating produced by pouring the PVC plastisol on a rubber surface having longitudinal grooves in the streamwise direction with triangular cross-sections. The modulus of rigidity of the rubber surface was much greater than that of the plastisol. Walsh (1980) has reported that similar grooved surfaces exposed to the flow have slightly reduced drag in air flows. In the (y, z)-plane the grooves had a height of 1.7 mm and a distance from apex to apex of 3.2 mm, which is equivalent to $50\nu/u_\tau$ at a towing speed of 40 cm/s. After gelling, the plastisol formed a flat surface of a depth 0.5 mm above the rubber surface apexes. The anisotropic coating had approximately the same onset

velocity for the static-divergence waves as an isotropic coating having the same average depth. However, the underlying longitudinal grooves did appear to modulate the wave amplitude along their crests. The spanwise wavelength was the same as the distance between the apexes. Consequently, the measurements of the wave amplitude and wavelength were not as reliable for the anisotropic coating.

5. Concluding remarks

The interaction of different compliant coatings with laminar, transitional and turbulent boundary layers has been investigated. A series of coatings were constructed with different thicknesses and shear moduli of rigidity and they were tested over a range of velocities. The lowest characteristic propagation velocity within the solid is that of transverse shear waves. Whenever the freestream velocity of the fluid was slightly larger than the transverse-wave speed within the solid, large-amplitude static-divergence waves appeared on the surface of the solid. These waves were apparently the result of a hydroelastic instability and only appeared under turbulent regions after the freestream exceeded a unique onset-velocity threshold. The onset velocity increased as the depth of the coating decreased.

In the present investigation, the static-divergence waves never appeared under a laminar boundary layer, even though laminar boundary layers were examined with freestream speeds of over twice the corresponding onset velocity for the turbulent case. However, using a fluid with sufficiently large viscosity, Hansen & Hunston (1983) were able to observe static-divergence waves in laminar flow on a rotating disk for rotational speeds of 1.6 times the observed onset speed for the turbulent case. Differences in results obtained from our facilities and those reported by Hansen & Hunston are not unexpected, owing to the significant differences in the experimental arrangement. However, these different results suggest that the onset velocity is not uniquely described by the external flow velocity. The differences emphasize the fact that further clarification of the parameters controlling the onset of the waves are direly needed to understand the interactions between the solid and the fluid.

In laminar and turbulent flowfields with freestream speeds below the onset velocity, the compliant coating had no measured effect on the boundary-layer structure. Thus no significant interaction appears to be occurring between the coating and the flowfields. Above the onset velocity, static-divergence waves appeared to act as roughness elements on the surface. Since they only appeared whenever a turbulent flow already existed, they were unable to trip turbulence in a laminar region, as seen in figure 10. Static-divergence waves never appeared immediately under a turbulent region, but the amplitude growth had a time constant of the order of the relaxation time of the solid.

When the static-divergence waves existed, their amplitude was always of the order of the coating thickness. For the thicker coatings, the amplitudes were 20–40 % of the undisturbed boundary-layer thickness. Consequently, the observed boundary layer over the waves increased up to 100 % in thickness, which is comparable to known results for rigid roughness elements. The phase velocity of the waves was typically less than $0.05U_\infty$. As the freestream velocity increased, the waves became less two-dimensional and developed larger variations in their amplitude along their crests. This disturbance seemed to lead to the formation of additional waves having a shorter span.

An examination of the dispersion curves for free-surface waves suggests that no significant interactions will occur for flow speeds below the transverse phase speed,

since no free-surface waves exist below this speed, but that ample opportunity exists for interactions for speeds well above the transverse phase speed. However, static-divergence waves appear for towing speeds somewhat above the transverse phase speed, which limits the possibilities for other interactions to occur. It appears important that additional experiments be conducted at speeds above the transverse phase speed but below the onset speed for static divergence. There is the possibility that some interaction between the fluid and the solid might occur in this range. It also appears important to develop methods to either suppress or delay the static-divergence waves, again in order to allow other interactions to occur.

If the coatings are to be used to reduce the drag on the surface, the static-divergence waves must be eliminated or mitigated. Obviously the coatings can be designed so that their characteristic velocities are sufficiently greater than those of the fluid; however, it is difficult to conceive how they could favourably interact with the fluid. In experiments with subsonic air flow over compliant surfaces, Ash (private communication) was able to suppress the static-divergence waves by covering the compliant surface with a thin, tightly stretched layer of Mylar. While suppressing the static-divergence waves, this also reduced the dynamic response of the surface (see Fischer *et al.* (1975), who report on Ash's experiments but do not describe static divergence). The theoretical work of Landahl (1962), Benjamin (1964) and Duncan *et al.* (1982) has suggested that the existence of these waves depends on the coating being viscoelastic; i.e. a strictly elastic solid would not be able to support the waves. Hence the response time of the coating becomes a critical parameter. Another solid, with similar elastic properties but a vastly different response time, should respond differently and may show significant interactions.

Some preliminary attempts were made in the present investigation to modify the static-divergence-wave mechanism. An anisotropic compliant coating was produced by pouring plastisol on a rubber surface having longitudinal grooves in the streamwise direction with triangular cross-sections. The only significant difference was that the amplitude of the static-divergence waves was modulated in the spanwise direction by the underlying grooved surface. Tests were also conducted in a 50 p.p.m. Polyox WSR-301 polymer solution. Visual observations showed that the amplitude of the static-divergence waves was reduced. Consequently the large increase in boundary-layer thickness was also considerably reduced so that it was only 10–40 % larger than the rigid-wall boundary layer. The polymer did not appear to alter the onset velocity of the waves.

This work is sponsored by the U.S. Office of Naval Research, under Contract N00014-81-C-0453. The continuous support of the program monitor, Dr M. M. Reischman, is greatly appreciated. The authors would like to acknowledge the valuable help of J. Caraher, M. Cooper, R. Cooper, J. Duncan, R. J. Hansen, D. L. Hunston, A. Kalnins, P. S. Klebanoff, H.-T. Liu and R. Srnsky. A shorter version of this work has appeared in the proceedings of the IUTAM Symposium on Structure of Complex Turbulent Shear Flow (Gad-el-Hak, Blackwelder & Riley 1982).

REFERENCES

Benjamin, T. B. 1960 Effects of a flexible boundary on hydrodynamic stability. *J. Fluid Mech.* **9**, 513.

Benjamin, T. B. 1963 The threefold classification of unstable disturbances in flexible surfaces bounding inviscid flows. *J. Fluid Mech.* **16**, 436.

BENJAMIN, T. B. 1964 Fluid flow with flexible boundaries. In *Proc. 11th Intl Congr. Appl. Mech., Munich* (ed. H. Görtler), p. 109. Springer.

BETCHOV, K. 1960 Simplified analysis of boundary-layer oscillations. *J. Ship Res.* **4**, 37.

BLACKWELDER, R. F. & KAPLAN, R. E. 1976 On the wall structure of the turbulent boundary layer. *J. Fluid Mech.* **76**, 89.

BOGGS, F. W. & HAHN, E. R. 1962 Performance of compliant skins in contact with high velocity flow in water. In *Proc. 7th Joint Army–Navy–Air Force Conf. on Elastomer Research and Development, San Francisco*, vol. 2, p. 443. U.S. Office of Naval Research.

BUSHNELL, D. M., HEFNER, J. N. & ASH, R. L. 1977 Effect of compliant wall motion on turbulent boundary layers. *Phys. Fluids Suppl.* **20**, S31.

CLAUSER, F. H. 1956 The turbulent boundary layer. *Adv. Appl. Mech.* **4**, 1.

CORINO, E. R. & BRODKEY, R. S. 1969 A visual investigation of the wall region in turbulent flow. *J. Fluid Mech.* **37**, 1.

DUNCAN, J. H., WAXMAN, A. M. & TULIN, M. P. 1982 Dispersion relationships for waves at the interface between a single layer visco-elastic compliant coating and a turbulent flow. *Hydronautics Tech. Rep.* 8111–1.

FALCO, R. E. 1977 Coherent motions in the outer region of turbulent boundary layers. *Phys. Fluids Suppl.* **20**, S124.

FISCHER, M. C. & ASH, R. L. 1974 A general review of concepts for reducing skin friction, including recommendations for future studies. *NASA Tech. Memo.* X-2894.

FISCHER, M. C., WEINSTEIN, L. M., BUSHNELL, D. M. & ASH, R. L. 1975 Compliant wall turbulent skin friction reduction reasearch. *AIAA 8th Fluid and Plasma Dyn. Conf., Hartford, CT; Paper* 75–833.

GAD-EL-HAK, M., BLACKWELDER, R. F. & RILEY, J. J. 1981 On the growth of turbulent regions in laminar boundary layers. *J. Fluid Mech.* **110**, 73.

GAD-EL-HAK, M., BLACKWELDER, R. F. & RILEY, J. J. 1982 Interaction of compliant surfaces with transitional and turbulent boundary layers. In *Proc. IUTAM Symp. on Structure of Complex Turbulent Shear Flow, Marseille* (ed. R. Dumas & L. Fulachier), p. 20. Springer.

HANSEN, R. J. & HUNSTON, D. L. 1974*a* An experimental study of turbulent flows over compliant surfaces. *J. Sound Vib.* **34**, p. 297.

HANSEN, R. J. & HUNSTON, D. L. 1974*b* An experimental study of the hydrodynamic drag on compliant surfaces: fluid property effects. In *Proc. 8th Intl Cong. Acoust.*, vol. 2, p. 579. Inst. Sound & Vib. Res., Southampton University.

HANSEN, R. J. & HUNSTON, D. L. 1976 Further observations on flow-generated surface waves in compliant surfaces. *J. Sound Vib.* **46**, 593.

HANSEN, R. J. & HUNSTON, D. L. 1983 Fluid-property effects on flow-generated waves on a compliant surface. *J. Fluid Mech.* **133**, 161.

HANSEN, R. J., HUNSTON, D. L., NI, C. C. & REISCHMAN, M. M. 1980*a* An experimental study of flow-generated waves on a flexible surface. *J. Sound Vib.* **68**, 317.

HANSEN, R. J., HUNSTON, D. L., NI, C. C., REISCHMAN, M. M. & HOYT, J. W. 1980*b* Hydrodynamic drag and surface deformations generated by liquid flows over flexible surfaces. In *Viscous Flow Drag Reduction* (ed. G. R. Hough), p. 439. AIAA Prog. Astro. Aero., vol. 72.

HOYT, J. W. 1981 A flow-visualization study of turbulent spots on solid and compliant surfaces. In *Proc. 7th Symp. Turbulence, Rolla, Missouri* (ed. J. L. Zakin & G. K. Patterson), p. 32–1.

JAEGER, J. C. & COOK, N. G. W. 1976 *Fundamental of Rock Mechanics*, 2nd edn, p. 314. Chapman & Hall.

KAPLAN, R. E. 1964 The stability of laminar incompressible boundary layers in the presence of compliant boundaries. Sc.D. thesis, MIT.

KLINE, S. J., REYNOLDS, W. C., SCHRAUB, F. A. & RUNSTADLER, P. W. 1967 The structure of turbulent boundary layers. *J. Fluid Mech.* **30**, 741.

KOVASZNAY, L. S. G., KIBENS, V. & BLACKWELDER, R. F. 1970 Large-scale motion in the intermittent region of a turbulent boundary layer. *J. Fluid Mech.* **41**, 283.

KRAMER, M. O. 1957 Boundary layer stabilization by distributed damping. *J. Aero. Sci.* **24**, 283.

KRAMER, M. O. 1962 Boundary layer stabilization by distributed damping. *J. Am. Soc. Nav. Engrs* **74**, 341.

LANDAHL, M. T. 1962 On the stability of laminar incompressible boundary layer over a flexible surface. *J. Fluid Mech.* **13**, 609.

LANDAU, L. D. & LIFTSHITZ, E. M. 1970 *The Theory of Elasticity.* Pergamon.

LISSAMAN, P. B. S. & HARRIS, G. L. 1969 Turbulent skin friction on compliant surfaces. *AIAA 7th Aerospace Sci. Meeting, New York; Paper* 69–164.

LIU, H.-T., KATSAROS, K. B. & WEISSMAN, M. A. 1982 Dynamic response of thin-wire wave gauges. *J. Geophys. Res.* **87**, 5686.

MCMICHAEL, J. M., KLEBANOFF, P. S. & MEASE, N. E. 1980 Experimental investigation of drag on a compliant surface. In *Viscous Flow Drag Reduction* (ed. G. R. Hough), p. 410. AIAA Astro. Aero., vol. 72.

ORSZAG, S. H. 1979 Prediction of compliant wall drag reduction. *NASA Contractor Rep.* 3071.

PURYEAR, F. W. 1962 Boundary layer control – drag reduction by use of compliant coatings. *David Taylor Model Basin Rep.* 1668.

RAYLEIGH, F. 1887 On waves propagated along the plane surface of an elastic solid. *Math. Soc. Proc. Lond.* **17**, 3.

SMITH, R. L. & BLICK, E. F. 1969 Skin friction of compliant surfaces with foamed material substrate. *J. Hydronaut.* **3**, 100.

WALSH, M. J. 1980 Drag characteristics of V-groove and transverse curvature riblets. In *Viscous Flow Drag Reduction* (ed. G. R. Hough), p. 168. AIAA Prog. Astro. Aero., vol. 72.

WEAVER, D. S. & UNNY, T. E. 1970 The hydroelastic stability of a flat plate. *Trans. ASME* E: *J. Appl. Mech.* **37**, 823.

WEAVER, D. S. & UNNY, T. E. 1973 On the dynamic stability of fluid-conveying pipes. *Trans. ASME* E: *J. Applied Mech.* **40**, 48.

WILLMARTH, W. W. & LU, S. S. 1972 Structure of the Reynolds stress near the wall. *J. Fluid Mech.* **55**, 65.